


RESEARCH ARTICLE

Stable ultrathin surfactant-free surface-engineered silicon nanocrystal solar cells deposited at room temperature

Vladimir Švrček¹ , Calum McDonald^{1,2}, Mickael Lozac'h¹, Takeshi Tayagaki¹, Tomoyuki Koganezawa³, Tetsuhiko Miyadera¹, Davide Mariotti² & Koji Matsubara¹

¹Research Center for Photovoltaics, National Institute of Advanced Industrial Science and Technology (AIST), Central 2, Umezono 1-1-1, Tsukuba, 305-8568, Japan

²Nanotechnology and Integrated Bio-Engineering Centre (NIBEC), Ulster University, Coleraine, UK

³Japan Synchrotron Radiation Research Institute (JASRI), 1-1-1, Kouto, Sayo-cho, Sayo-gun, Hyogo 679-5198, Japan

Keywords

Silicon nanocrystals, surfactant-free surface engineering, ultrathin film solar cells

Correspondence

Vladimir Švrček, Research Center for Photovoltaics, National Institute of Advanced Industrial Science and Technology (AIST), Central 2, Umezono 1-1-1, Tsukuba 305-8568, Japan.
E-mail: vladimir.svrcek@aist.go.jp

Funding Information

The GIWAXS measurement was performed at SPring-8 BL46XU with the approval of the Japan Synchrotron Radiation Research Institute (JASRI, proposal nos. 2015B1600 and 2015B1891). This work was partially supported by EPSRC (EP/K022237/1 and EP/M024938/1).

Received: 15 May 2017; Revised: 4 July 2017;
Accepted: 6 July 2017

Energy Science and Engineering 2017;
5(4): 184–193

doi: 10.1002/ese3.165

Introduction

Colloidal semiconductor nanoscale crystals, with quantum confinement, offer a powerful platform for a new generation of device engineering [1, 2]. Colloidal nanocrystals may be tailored in size, shape, and composition and their surfaces functionalized by diverse chemical approaches [3–7]. The quantum mechanical coupling of over hundreds to thousands of atoms varies the electronic structure, whereby the optical and magnetic properties of materials can be tuned leading to new phenomena [8, 9]. The energy band gap can be willingly tuned to emit and absorb photons in the broader spectral region in comparison

Abstract

We present a scalable technology at room temperature for the fabrication of ultrathin films based on surfactant-free surface-engineered silicon nanocrystals (SiNCs). Environmentally friendly pulsed fsec laser induced surface engineering of SiNCs and vacuum low-angle spray deposition is used to produce ultrathin films. Surface engineering of SiNCs improved stability and dispersibility of SiNCs by allowing thin (30 nm thickness) and exceptionally smooth (mean square roughness corresponds to 0.32 nm) film deposition at room temperature. The quality of the SiNC thin films is confirmed by ultrafast photoluminescence measurements and by applying such films for solar cells. We demonstrate that films produced with this approach yield good and stable devices. The methodology developed here is highly relevant for a very wide range of applications where the formation of high-quality ultrathin films of quantum dots with controllable thickness and smoothness is required.

to the bulk [1, 10]. In the last few years, the research on colloidal nanocrystals has moved from fundamental research to first applications in biology, optoelectronics, and photovoltaics [11–15].

In particular, sunlight to electricity conversion (e.g., photovoltaics) has undergone a spectacular drop in cost as a result of breakthroughs in material science, engineering, design, and manufacturing. The silicon-based solar cell market showed an exponential growth rate in the last 20 years [16]. It is believed that further significant improvements with bigger impact in solar cell efficiency are possible through so-called third-generation photovoltaic device architectures where the use of silicon-based

quantum dots or silicon nanocrystals (SiNCs) is particularly appealing [17]. Clearly opportunities exist through the precise control of the nanocrystal size which determines quantum confinement properties, through accurate control of the surface characteristics, and also through control of the distance between NCs. Desired surface properties can be achieved via surface engineering (with and without mechanical stress on surface), in particular, without the use of surfactants [18] and where the very large surface area to volume ratio can impinge on the overall NC behavior when it is accurately engineered without surfactants. Control of the NC size and surface properties determines the energy band gap of silicon to an optimal value (i.e., 1.6 eV), and allows precise design of absorbing layers for tandem solar cells [17, 19, 20]. Furthermore, quantum confinement can extensively improve efficiency (>40%) through enhanced inverse Auger recombination and the generation of multiple excitons (MEG) [21], while the large surface area can contribute not only to tuning the electronic properties of the nanocrystals, but also to controlling their interactions with the host matrix constituting a new class of hybrid quantum–material composites [22, 23].

In contrast to other semiconductor nanocrystals prepared by solution chemistry [24, 25], intrinsic and doped SiNCs can be synthesized simply and cheaply from low-cost materials (e.g., polycrystalline wafers) by an electrochemical etching approach [26]. As SiNCs can be in colloidal dispersion, solar cells or any optoelectronic device (e.g., light-emitting diodes) can be fabricated by various low-cost deposition techniques including simple one-step solution coating and spray procedures [27]. Indeed, various solar cell structures ranging from sensitized solar cells on mesoscopic semiconducting TiO_2 to the planar and bulk heterojunction architecture can be designed and produced [28]. However, to date, the impact of the SiNC size distribution at quantum confinement sizes on the film formation, and thus on the solar cell performance, has not been solved. Due to the large SiNC size distribution, a noncontinuous and rough film is usually obtained, where pinholes introduce shunting pathways limiting the solar cell performance [29]. On the other hand, maintaining a low temperature during deposition is also a crucial factor to avoid recrystallization of the SiNCs and to allow for device fabrication which involves temperature-sensitive materials (e.g., glass, polymer) [30].

Over the recent years, it has become necessary to deploy thin-film deposition methods for SiNCs suitably applicable to large area deposition, as wafers for the manufacture of optoelectronic devices and/or solar panels have become larger in size [31]. Furthermore, the development of devices with multilevel interconnects requires the surface of insulation films to be planarized, therefore surface

planarization techniques to form planar SiNC films can also become a necessity [32,33]. In an effort to satisfy these requirements, in general, for nanocrystal-based thin-film formation techniques at low temperatures, the aggregation of nanocrystals can be avoided by surface engineering [18]. In addition, plasma-induced surfactant-free surface chemistries on SiNCs showed encouraging results in terms of improved quality and stability of the SiNCs [18]. Surfactant-free femtosecond (fsec) laser-induced surface-engineered SiNCs also proved to be highly effective in promoting the separation of SiNCs [34], which largely contribute to preserve the individuality of the SiNCs during integration into thin films.

In this work, we employ pulsed fsec laser-induced surface engineering of colloidal SiNCs (produced by electrochemical etching, ~3 nm average diameter) together with low-angle spray deposition in vacuum to produce ultrathin films (<30 nm) of SiNCs for solar cells. We demonstrate that surface engineering of SiNCs induced by fsec laser allows the fabrication of smooth photoluminescent thin films with mean square roughness (Rms) corresponds to 0.32 nm. Photoluminescence dynamic studies confirm that the characteristic of the SiNCs are preserved throughout the surface engineering and film preparation steps. We show that the methodology developed here is highly relevant for a very wide range of applications where high-quality films of nanocrystals are required, and as an example it is demonstrated here for fabricating PV devices.

Experimental Details

Synthesis and Surface engineering of SiNCs

SiNCs were produced by electrochemical etching of Si wafer in HF followed by mechanical removal [26]. More specifically, SiNCs were produced by electrochemical etching of p-type Si wafers (HF:ethanol 1:4, constant current 20 mA/cm²) for 1 h, which yields SiNC agglomerates. The fsec laser treatment is used for both SiNC deagglomeration and simultaneous surface passivation [34]. In particular, 5 mg of SiNC powder (i.e., SiNC agglomerates) from the electrochemical etching process was transferred into 5 mL ethanol. The fsec laser irradiation [34] used a wavelength of 400 nm and a pulse width 100 fsec. A barium borate (BBO) crystal was used to select 400 nm. During the irradiation, the glass container was rotated. The process was conducted at room temperature and for 30 min. The laser beam was shaped and focused onto a spot (2 mm in diameter) on the liquid surface by an optical lens with a focal length of 250 mm. The average laser power was set to be approximately 30 mW while using the repetition rate of 1 kHz. In order to check the

efficiency of the laser-based surface engineering process with simplified experimental conditions and larger absorption profile of chosen wavelength we first compare with our previous works [34]. Similar to our previous studies, we clearly confirmed the trends in stability and an increase in the PL intensity after fsec laser processing after simplified experimental conditions.

Low-angle spray deposition

The colloids of SiNCs treated by the laser process were then deposited using the deposition system depicted in the schematic diagram of Figure 1 without any further step or filtration. This apparatus consists of a colloidal solution tank, stopper valve placed after the tank, and a spray nozzle. The IOTA ONE (Parker Hannifin Corporation, East Pine Brook, NJ, USA) valve driver for high-speed solenoid valves was used to control automatically the valve. The valve was used to perform pulsed deposition by stop/start action and by controlling the time interval. The pulse duration for the valve was set at 0.5 sec open and 1 sec closed, and repeated 30 times until the 5 mL colloidal SiNCs/ethanol dispersion was fully consumed. During deposition, the pressure in the chamber increased from 2×10^{-5} Torr to 10^{-2} Torr. The actual sample preparation was done at room temperature on quartz or glass/indium-doped tin oxide (ITO)/compact-TiO₂/mesoporous-TiO₂ substrates resulting in a thickness of about 30 nm.

Fabrication of solar cell devices

Figure 2 represents schematics cross-section of solar cell structure. Glass substrates with patterned indium-tin-oxide (ITO) were cleaned by O₂ plasma. The TiO₂ compact blocking layer was formed by dissolving titanium (IV)

isopropoxide and triethanolamine in ethanol, stirred for 2 h at 40°C, and then left for 24 h. The solution was spin coated at 5000 revolution per minute (rpm) for 30 sec and then annealed at 400°C in a furnace for 2 h. The mesoporous TiO₂ layers were deposited by spin coating (2000 rpm for 60 sec) a solution of commercial dyesol 18-NRT titania nanoparticle paste dissolved in ethanol in a 1:2 ratio of paste to ethanol. The films were then annealed again in a furnace at 400°C for 2 h. Then by low-spray angle deposition at room temperature, 30-nm thick film of fsec laser surface-engineered SiNCs was deposited (Fig. 2B). The hole transport layer was prepared by dissolving 0.207 g of 2,2',7,7'-Tetrakis[N,N-di(4-methoxyphenyl)amino]-9,9'-spirobifluorene (Spiro-MeOTAD, Sigma-Aldrich, St. Louis, MO, USA) in 1 mL chlorobenzene and deposited by spin coating at 3000 rpm for 30 sec. Silver metal contacts were deposited by thermal evaporation using a shadow mask. The resulting device active area was 0.04 cm².

Power conversion efficiency

Solar simulated AM 1.5G sunlight was generated using Wacom Electric Co. solar simulator (JIS, IEC standard conforming, CLASS AAA, Wacom, Taito-Ku, Tokyo, Japan) calibrated to give 100 mW/cm² using a silicon reference cell. The electrical data were recorded using a Keithley 2400 source meter (Tektronix, Inc., Beaverton, OR, USA). Devices were measured in the range -0.1 to 0.6 V with scan rates between 150 and 1500 mV/sec.

External quantum efficiency

The solar cell external quantum efficiency (EQE) characteristics were measured under illumination using an Air Mass 1.5 Global (AM1.5G) with light intensity calibrated to 100 mW/cm² by using a reference cell for a-Si solar cells.

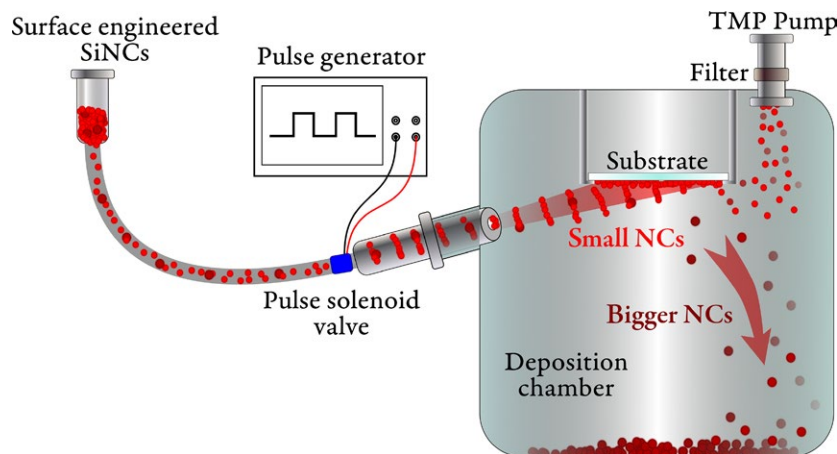


Figure 1. Schematic diagram of the deposition system used to produce ultrathin surface-engineered silicon nanocrystal (SiNC) films; the system uses a homemade pulsed spray system where the speed of the solenoid duration range was controlled automatically by an IOTA ONE (Parker) valve driver.

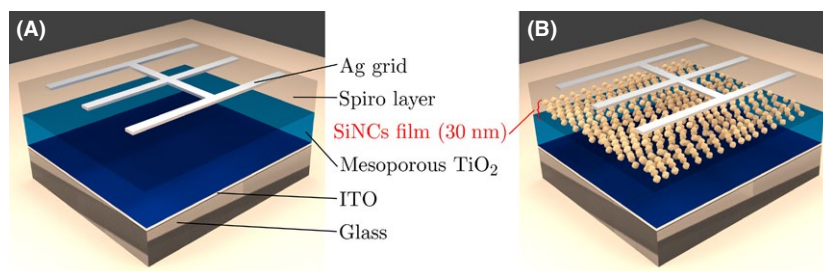


Figure 2. (A) Schematics showing cross-section of reference solar cell structure and (B) solar cells with ultrathin film of surface-engineered silicon nanocrystals (SiNC).

Photoluminescence and PL decay measurements

The photoluminescence (PL) was measured by a spectrometer (Spectrofluorometer, Horiba Jobin Yvon, Palaiseau, France) at room temperature with excitation at 375 nm. Time-resolved PL spectra were measured using a streak camera with the second harmonics of a Ti:sapphire laser (400 nm) as an excitation light source.

XRD analysis

The X-ray diffraction (XRD) measurements of thin films were performed with a synchrotron radiation (SPRING-8) at the beam line BL46XU. The film was mounted on the goni stage (HUBER X-ray diffractometer) to allow XRD analysis. GIWAXS data were acquired using 12.398 keV X-rays ($\lambda = 1.000 \text{ \AA}$) at an incident angle of 0.25° and diffracted X-rays were captured at 1.0 sec intervals by a two-dimensional detector (PILATUS 300K, DECTRIS, Baden-Daettwil, Switzerland) located at a distance of $L = 174.5 \text{ mm}$ from the sample.

Thickness and surface analysis

The atomic force microscopy (AFM) measurements (Nano/ Navi, E-SWEEP SII Nanotechnology) on SiNC ultrathin films on quartz substrate were performed either with contact or with tapping mode. Dektak-XT (Bruker, Kanagawa, Japan) and AFM was used to evaluate the thickness of the deposited thin film on a quartz substrate and a corresponding thickness of 30 nm from the step size was evaluated. The AFM image analysis was carried out using commercial software procedures to determine the surface roughness.

Experimental Results and Discussion

Luminescence properties of ultrathin SiNCs films

The steady-state photoluminescence and time-resolved photoluminescence have been recognized to be useful tools

to understand charge extraction in thin film solar cells; therefore, we first looked into the charge dynamics of surface-engineered SiNCs directly in colloidal solution and after SiNC ultrathin film deposition on quartz substrate

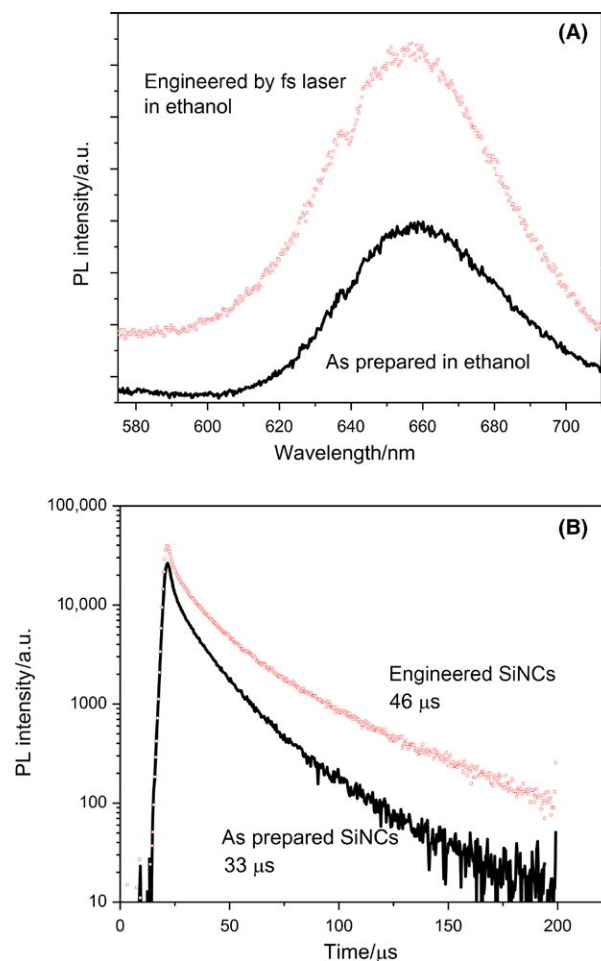


Figure 3. (A) Time-gated photoluminescence (PL) shows a broad spectra spanning from 600 to 750 nm for as-prepared SiNCs dispersed in ethanol (black line) and fs laser processed SiNCs (red symbols) also in ethanol, both measured directly in colloid with excitation at 400 nm. (B) PL decays corresponding to PL emission in (A).

by low-angle deposition techniques. Figure 3A shows the time-gated PL spectra (400 nm excitation) for as-prepared SiNCs dispersed in ethanol and for SiNCs processed by fsec laser in ethanol, where both samples were dispersed in ethanol for same time duration. The time-gated PL is broad, spanning from 600 to 750 nm; however, it evolves on the μsec timescale (Fig. 3B) from a band centered around 660 nm. The PL peak exhibits an increase in intensity for surface-engineered SiNCs. Corresponding PL decays on the μsec timescale are shown in Figure 3B. The PL decay time is extended by a few tens of microsecond in the fsec laser-processed sample compared to as-prepared SiNCs, which underline higher quality SiNCs after laser processing. The μsec transition can originate from the relaxation of the excited electrons in the SiNC core to the lower states, or from trapping by defect states on the surface which are reduced under surface engineering. As a result, the PL peak exhibits an increase in intensity for surface-engineered SiNCs. The PL decay is in the microseconds range which suggests that the nature of the transition is most likely indirect. The decay constants were determined by fitting the experimental data with a single exponential function in the 100–200 nsec region. Our results indicate that the PL decay constant after surface engineering increased from 33 to 46 μsec .

Next, surface-engineered SiNCs were used to fabricate ultrathin films by low-angle spray deposition on quartz substrates at room temperature. Figure 4 shows a typical AFM image of the deposited SiNCs (exposed to air). Such SiNC thin films exhibit a very smooth surface morphology. The analyzed surface has an area of $200 \times 200 \text{ nm}^2$ and the evaluated Rms corresponds to 0.32 nm.

The samples were then analyzed by grazing incidence wide-angle X-ray scattering (GIWAXS). Figure 5A shows GIWAXS pattern of SiNCs for ultrathin films represented in reciprocal lattice space. The XRD broad spectrum (Fig. 5B) of the SiNCs film evaluated from the GIWAXS pattern confirms the presence of the SiNCs in the ultrathin films, where the broadening is ascribed to the quantum confinement size of the SiNCs whereby the general expression for the line broadening is given by Williamson and Hall [35]. The characteristic diffraction lines are broadened and their width differs by variation of grazing incidence angle indicating the variation of nanocrystals sizes [36].

Figure 6A shows typical time-gated PL spectra of the 30-nm thick film on quartz substrate. The PL maxima (Fig. 6B) is located at 630 nm, which is slightly shifted in comparison to the PL emission of the corresponding colloid (Fig. 3A). This 30 nm blue shift is most likely due to the deposition approach, which selectively deposit the smallest SiNCs (see Fig. 1). However, the PL dynamics of the SiNCs in the films is the same as for the colloids (Fig. 3B) with a decay constant of about 43 μsec (Fig. 6C).

Although the exact nature is still debated, PL in SiNCs is often associated to quantum confinement [37, 38]. In addition, several works point out and attribute the luminescence emission to the variable structures of the samples and the many possible defect states in SiNCs mostly localized at the SiNC surface [39]. Figure 7A shows typical time-gated PL spectrum of the 30-nm thick film on quartz substrate at excitation $10^{-1} I_0$ ($I_0 \wedge 1 \text{ kJ/cm}^2$), while Figure 7B shows the PL spectra as a function of the wavelength at different excitation intensities

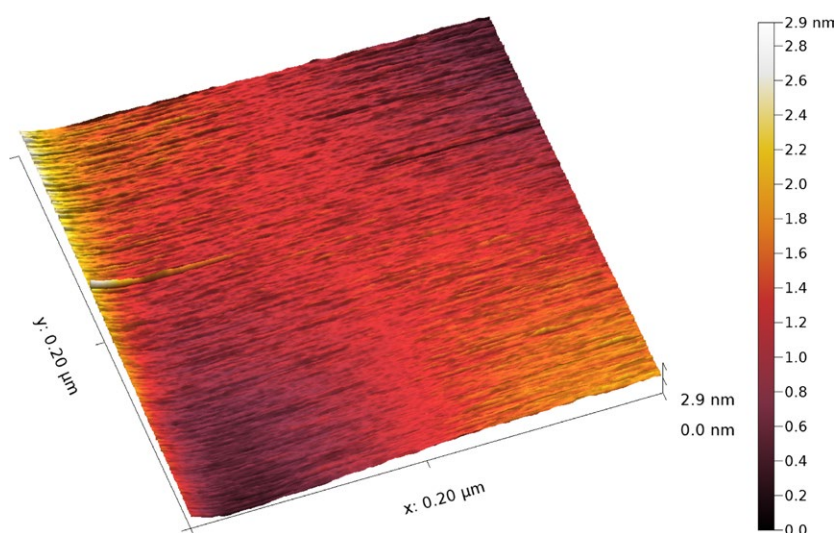


Figure 4. Typical AFM image of the SiNCs thin film with thickness 30 nm deposited at low angle and room temperature. The analyzed surface has an area of $200 \times 200 \text{ nm}^2$ and the evaluated mean square roughness (Rms) corresponds to 0.32 nm.

corresponding to I_0 , $10^{-0.3} I_0$, $10^{-0.5} I_0$, $10^{-1} I_0$, $10^{-2} I_0$. The inset in Figure 7B plots the PL intensity as a function of excitation intensity and Figure 7C presents respective PL decays whereby the legend summarizes the corresponding decay constants. It is well accepted that the size of the SiNCs is the key factor to determining the ratio of zero-phonon transitions to phonon-assisted transitions [40, 41]. On the other hand, the state-filling effect is closely linked to the recombination rate and consequently high recombination rate leads to a shortening of the lifetime at decreased excitations intensities. However, we observe no significant changes in the decay constants, thus suggesting that the state-filling effect is not significant [42]. Furthermore, the PL results suggest that in surface-engineered SiNCs the state-filling effect can effectively prevent hot carriers from being thermalized quickly. Due to the indirect gap of crystalline silicon, a thermalization relaxation time of SiNCs is about 1000 times slower than common carrier cooling rates in bulk semiconductors [43]. Since Auger recombination is proportional to the cube of the carrier density and, initially, a large population of carriers is pumped at higher excitation intensities (comparable to solar irradiation), we should expect Auger recombination to occur at an accelerated rate, possibly eased also by a lower defect state density of surface-engineered SiNCs that present reduced non-radiative recombination paths.

Photovoltaic applications of ultrathin films based on doped SiNCs

The PL studies suggest that such thin films with high quality of highly packed SiNCs could be advantageous for carrier multiplication in SiNCs and photovoltaic applications [44, 45]. In order to test the photovoltaic properties of the ultrathin SiNCs films, we fabricated solar cells. The photovoltaic properties of the typical solar cell based on the ultrathin film of SiNCs deposited at similar conditions are shown in Figure 8. Silver (Ag) was used as the top electrode and ITO as the bottom electrode. Figure 8A and B show the current density–voltage (J – V) curves of the SiNC solar cell device (ITO/compact-TiO₂/mesoporous-TiO₂/SiNCs/spiro-OMeTAD/Ag) and the control solar cell device (ITO/compact-TiO₂/mesoporous-TiO₂/spiro-OMeTAD/Ag) in the dark and under illumination. As can be seen from the results, the control device exhibits a negligible PV effect (Fig. 8B), while a considerable PV output emerges after the introduction of an ultrathin surface-engineered SiNCs layer (Fig. 8A). As it is shown in Figure 8A, the SiNCs solar cell has an open-circuit voltage (V_{oc}) and short-circuit current density (J_{sc}) of 0.42 V and 112 mA/cm², respectively, with a corresponding power conversion efficiency of 0.0096% and a fill factor

of 20%. We also measured the EQE of the corresponding cells, which are compared in Figure 8C. From the overall EQE it is evident that a broad range of incident light from 300 to 600 nm can be harvested to generate electric power, thereby validating the contribution of the ultrathin film made of surface-engineered SiNCs.

The inset in Figure 8C shows the schematic band diagram of the device with SiNCs. The band alignment without a potential barrier ensures an efficient charge transport to their respective ohmic contacts. In our case the charge carriers are separated most likely between TiO₂ (electrons) and SiNCs (holes). The TiO₂ layer acts as a selective carrier transport that provides an excellent hole blocking layer [46, 47]. The photogenerated hole carriers in SiNCs are separated efficiently by using p-type doped SiNCs. Electron and hole separation between TiO₂ and

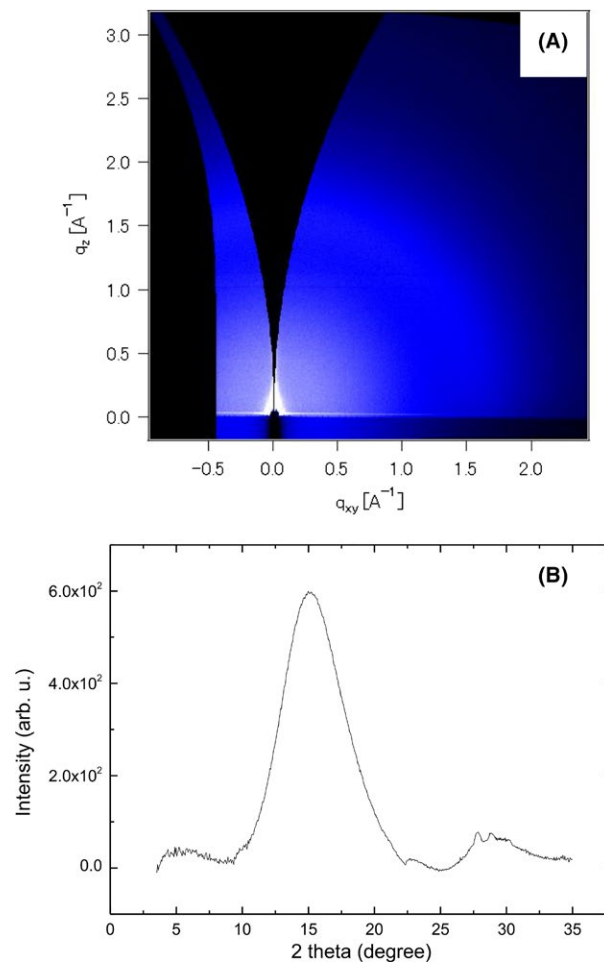


Figure 5. (A) Grazing incident wide-angle X-ray scattering (GIWAXS) patterns of surface-engineered SiNCs deposited by low-angle spray deposition, represented in reciprocal lattice space. (B) XRD spectrum corresponding to figure (A).

SiNCs is crucial for the open-circuit voltage (V_{oc}) by preventing charge recombination and enabling an efficient extraction even at low electric field (Fig. 8A). Another crucial factor concerns the nanocrystal surface chemistry. We believe that the charge carrier separation at SiNCs interface is deeply related to the fabrication process by laser engineering that allows a refinement of the nanocrystal surface chemistry. Indeed, nonradiative recombination at dangling bond sites may be responsible for the emission quenching due to poorly passivated SiNCs. Therefore, the high intensity from the PL spectra of our films as shown in Figure 6B underlines a low concentration of dangling

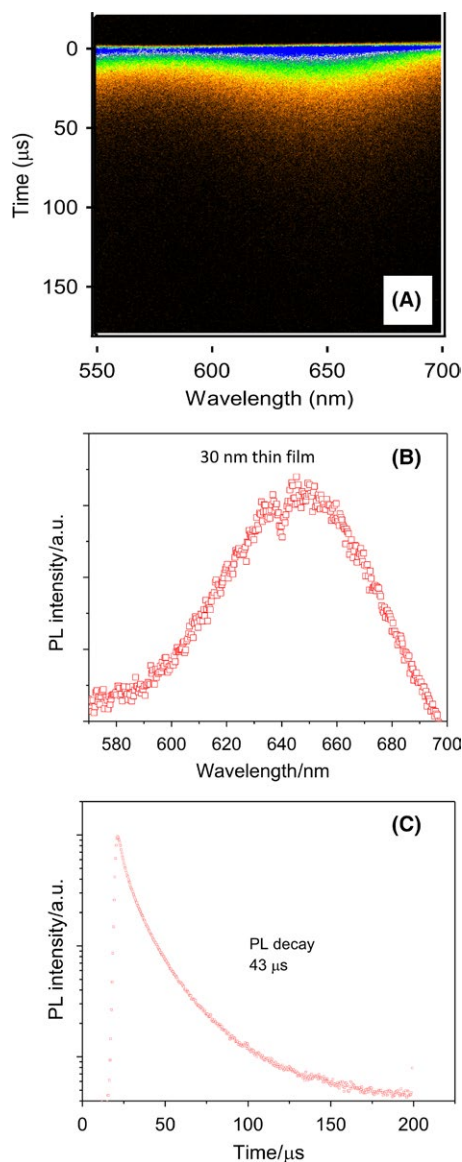


Figure 6. (A) Time-gated PL spectra of the 30-nm thick film on quartz substrate. (B) PL spectrum at room temperature. (C) PL decay corresponding to (B).

bonds that indirectly supports the effective charge separation present in our devices.

The improved PL decay due to surface-engineered SiNCs may be closely related to a lower interfacial barrier and a more efficient charge carrier extraction as discussed above, thus contributing to an enhancement of photovoltaic properties, such as reduced hysteresis (Fig. 9). In Figure 9A we show J–V curves for the best-performing solar cell devices in forward and reverse scans with the scan rate of 150 mV/sec. The champion ultrathin SiNC device achieved, in the reverse scan, a power conversion efficiency of 0.016% with a short-circuit current density

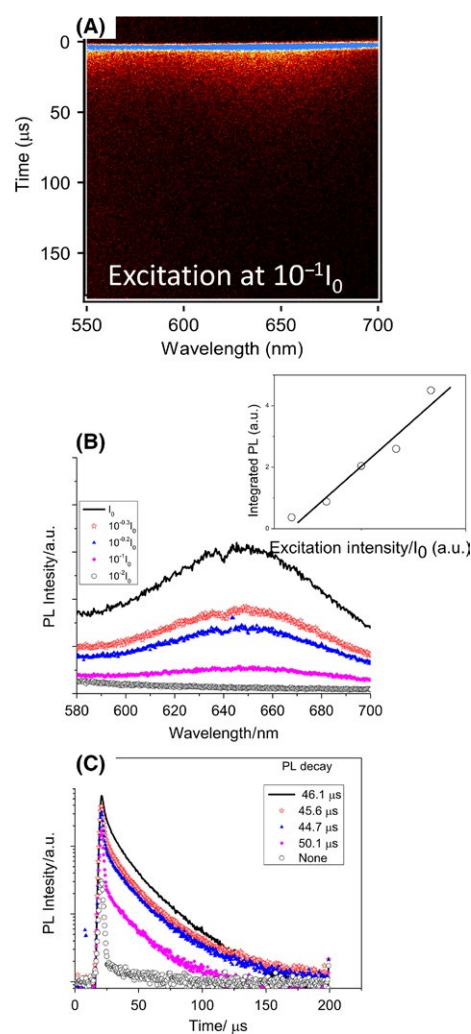


Figure 7. (A) Typical time-gated photoluminescence (PL) spectrum of the 30-nm thick film on quartz substrate at excitation $10^{-1}I_0$. (B) The PL spectra as a function of the wavelength at different excitation intensities: I_0 , $10^{-0.3}I_0$, $10^{-0.5}I_0$, $10^{-1}I_0$, $10^{-2}I_0$. The inset in (B) plots PL intensity as a function of excitation intensity. (C) PL decays whereby the legend summarizes evaluated decay time constants.

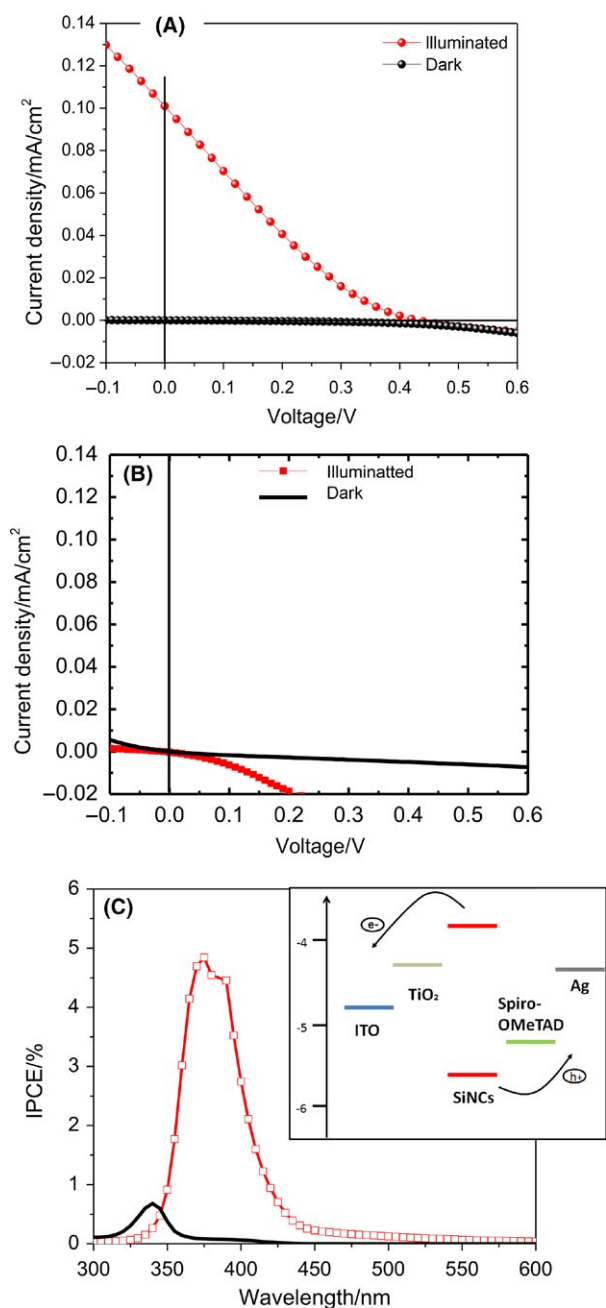


Figure 8. (A) Current density–voltage characteristic for a SiNC solar cell (red symbols) and (B) for the same structure without SiNCs. (C) External quantum efficiency (EQE) as a function of the wavelength for corresponding solar cells is plotted. Inset in (C) shows the schematic band diagram of the solar cell with SiNCs.

(J_{SC}) of 0.12 mA/cm², open-circuit voltage (V_{OC}) of 0.43 V. Device stability is another major concern with regard to practical applications. Therefore, we recorded the device performance after 3 months with devices stored in air and ambient conditions. The solar cells are very stable at room temperature as illustrated in Figure 9B. We show

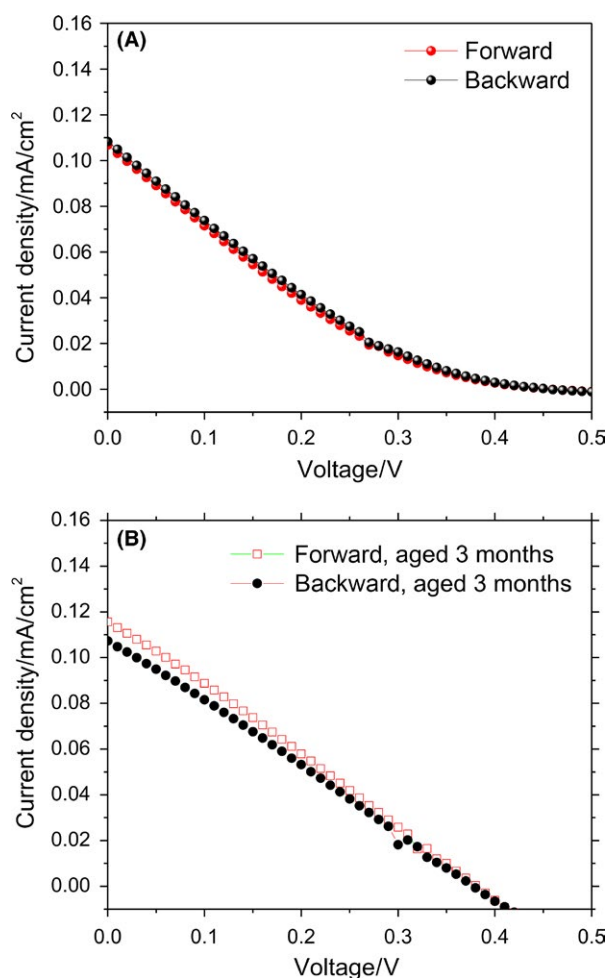


Figure 9. (A) Current density–voltage characteristic for silicon nanocrystal solar cells. (B) Current density–voltage characteristic of the devices after 3 months stored in air and ambient conditions.

both J–V curves of solar cell in forward and reverse scans that confirms also a low hysteresis is maintained after aging.

Conclusions

The PL and photovoltaic properties of silicon nanocrystals (SiNCs) 30-nm thick and smooth ultrathin films have been investigated. A technological approach to fabricate SiNC thin films is proposed and based on the combination of surface engineering by fs laser irradiation and low-angle SiNCs deposition. The longer lifetime in the PL emission band is likely attributed to the nature of the surface chemistry, which has been largely improved by the laser-based process. We demonstrate that the PL decay properties are preserved during the room-temperature deposition. The surface engineering step together with the production of thin films has allowed the

fabrication of prototype transparent solar cells. The low-temperature deposition approach provides great flexibility, whereby the concepts discussed in this work can be also expanded to other ultrathin nanocrystal solar cells based on different material systems at low cost.

Acknowledgments

The GIWAXS measurement was performed at SPring-8 BL46XU with the approval of the Japan Synchrotron Radiation Research Institute (JASRI, proposal nos. 2015B1600 and 2015B1891). This work was partially supported by EPSRC (EP/K022237/1 and EP/M024938/1). The authors also acknowledge the support of the EU COST Action TD1208.

Conflict of Interest

None declared.

References

- Rogach, A. 2008. Semiconductor nanocrystal quantum dots: synthesis, assembly, spectroscopy and applications. Springer, Wien.
- Delerue, C. 2016. Nanocrystal solids: Order and progress. *Nat. Mater.* 15:498–499.
- Shevchenko, E. V., M. I. Bodnarchuk, M. V. Kovalenko, D. V. Talapin, R. K. Smith, S. Aloni et al. 2008. Nanoparticles with different functionalities and their periodic structures. *Adv. Mater.* 20:4323–4329.
- Talapin, D. V., J. H. Nelson, E. V. Shevchenko, S. Aloni, B. Sadtler, and A. P. Alivisatos. 2007. Seeded Growth of Highly Luminescent CdSe/CdS Nano-Heterostructures with Rod and Tetrapod Morphologies. *Nano Lett.* 7:2951–2959.
- Xu, W., P. Jain, B. Beberwyck, and A. P. Alivisatos. 2012. Probing Redox Photocatalysis of Trapped Electrons and Holes on Single Sb-doped Titania Nanorod Surfaces. *J. Am. Chem. Soc.* 134:3946–3949.
- Liu, W. Y., A. Y. Chang, R. D. Schaller, and D. V. Talapin. 2012. Colloidal InSb nanocrystals. *J. Am. Chem. Soc.* 134:20258–20261.
- Kagan, C. R., and C. B. Murray. 2015. Charge transport in strongly coupled quantum dot solids. *Nat. Nanotechnol.* 10:1013–1026.
- Talapin, D. V., and C. B. Murray. 2005. PbSe Nanocrystal Solids for n- and p-Channel Thin Film Field-Effect Transistors. *Science* 310:86–89.
- Klimov, V. I., S. A. Ivanov, J. Nanda, M. Achermann, I. Bezel, J. A. McGuire et al. 2007. Single-exciton optical gain in semiconductor nanocrystals. *Nature* 447:441–446.
- Murray, C. B., D. J. Norris, and M. G. Bawendi. 1993. Synthesis and characterization of nearly monodisperse CdE (E = sulfur, selenium, tellurium) semiconductor nanocrystallites. *J. Am. Chem. Soc.* 115:8706–8715.
- Kovalenko, M. V., L. Manna, A. Cabot, Z. Hens, D. V. Talapin, C. R. Kagan et al. 2015. Prospects of Nanoscience with Nanocrystals. *ASC Nano* 9:1012–1057.
- Kamat, P. V. 2012. Boosting the Efficiency of Quantum Dot Sensitized Solar Cells through Modulation of Interfacial Charge Transfer. *Acc. Chem. Res.* 45:1906–1915.
- Shirasaki, Y., G. J. Supran, M. G. Bawendi, and V. Bulovic. 2013. Emergence of Colloidal Quantum-Dot Light-Emitting Technologies. *Nat. Photonics* 7:13–23.
- Peteiro-Cartelle, J., M. Rodríguez Pedreira, F. Zhang, P. Rivera-Gil, L. L. Mercato, and W. J. Parak. 2009. How colloidal nano- and microparticles could contribute to medicine - a personal perspective both from the eyes of physicians and materials scientists. *Nanomedicine* 4:967–979.
- Wang, Y., X. Li, J. Song, L. Xiao, H. Zeng, and H. Sun. 2015. All-Inorganic Colloidal Perovskite Quantum Dots: A New Class of Lasing Materials with Favorable Characteristics. *Adv. Mater.* 27:7101–7108.
- Fraunhofer, I. S. E. 2015. Current and Future Cost of Photovoltaics—Long-term Scenarios for Market Development, System Prices and LCOE of Utility-Scale PV Systems” (PDF). Available at <http://www.agora-energiewende.org/> [accessed on 01 February 2015]
- Green, M. A. 2003. Third generation photovoltaics. Springer, Berlin.
- Mariotti, D., V. Švrček, W. J. Hamilton, M. Schmidt, and M. Kondo. 2012. Silicon Nanocrystals in Liquid Media: Optical Properties and Surface Stabilization by Microplasma-Induced Non-Equilibrium. *Adv. Funct. Mater.* 22:954–964.
- Miles, R. 2006. Photovoltaic solar cells: Choice of materials and production methods. *Vacuum* 80:1090–1097.
- Luque, A., and S. Hegedus, eds. 2003. Handbook of photovoltaic science and engineering. John Wiley & Sons, Ltd., Chichester, UK.
- Nozik, J. 2008. Multiple exciton generation in semiconductor quantum dots. *Chem. Phys. Lett.* 457:3–11.
- Dirin, D. N., S. Dreyfuss, M. I. Bodnarchuk, G. Nedelcu, P. Papagiorgis, G. Itskos et al. 2014. Lead Halide Perovskites and Other Metal Halide Complexes as Inorganic Capping Ligands for Colloidal Nanocrystals. *J. Am. Chem. Soc.* 136:6550–6553.
- Švrček, V., T. Yamanari, D. Mariotti, S. Mitra, T. Velusamy, and K. Matsubara. 2015. A silicon nanocrystal/polymer nanocomposite as a down-conversion layer in organic and hybrid solar cells. *Nanoscale* 7:11566–11574.
- Kopping, J. T., and T. E. Patten. 2008. Identification of Acidic Phosphorus-Containing Ligands Involved in the

- Surface Chemistry of CdSe Nanoparticles Prepared in Tri-N-octylphosphine Oxide Solvents. *J. Am. Chem. Soc.* 130:5689–5698.
25. Hassinen, A., I. Moreels, K. De Nolf, P. F. Smet, J. C. Martins, and Z. Hens. 2012. Short-chain alcohols strip X-type ligands and quench the luminescence of PbSe and CdSe quantum dots, acetonitrile does not. *J. Am. Chem. Soc.* 134:20705.
 26. Švrček, V., A. Slaoui, and J. C. Muller. 2004. Ex situ prepared Si nanocrystals embedded in silica glass: Formation and characterization. *J. Appl. Phys.* 95:3158–3164.
 27. Purkait, T. K., M. Iqbal, M. Amirul Islam, M. H. Mobarok, C. M. Gonzalez, L. Hadidi et al. 2016. Alkoxy-Terminated Si Surfaces: A New Reactive Platform for the Functionalization and Derivatization of Silicon Quantum Dots. *J. Am. Chem. Soc.* 138:7114–7120.
 28. Xin, X., J. Wang, W. Han, M. Ye, and Z. Lin. 2012. Dye-sensitized solar cells based on a nanoparticle/nanotube bilayer structure and their equivalent circuit analysis. *Nanoscale* 4:964–971.
 29. Velusamy, T., S. Mitra, M. L. Macias-Montero, V. Švrček, and D. Mariotti. 2015. Varying Surface Chemistries for p-Doped and n-Doped Silicon Nanocrystals and Impact on Photovoltaic Devices. *ACS Appl. Mater. Interfaces.* 7:28207–28214.
 30. Ito, M., C. Koch, V. Švrček, M. B. Schubert, and J. H. Werner. 2001. Silicon thin film solar cells deposited under 80°C. *Thin Solid Films* 383:129–131.
 31. Mason, T. L., A. Straub, D. Inns, D. Song, A. Aberle, and G. Armin. 2005. A Novel method for the development of Solar Energy. *Appl. Phys. Lett.* 86:V172108–172112.
 32. Doering, R., and Y. Nishi, eds. 2007. *Handbook of semiconductor manufacturing technology*, 2nd ed. CRC Press, Boca Raton, FL.
 33. Zhuang, Z., F. Huang, Z. Lin, and H. Zhang. 2012. Aggregation-Induced Fast Crystal Growth of SnO₂ Nanocrystals. *J. Am. Chem. Soc.* 134:16228–16234.
 34. Švrček, V., D. Mariotti, U. Cvelbar, G. Filipič, M. Lozac'h, C. McDonald et al. 2016. Environmentally Friendly Processing Technology for Engineering Silicon Nanocrystals in Water with Laser Pulses. *J. Phys. Chem. C* 120:18822–18830.
 35. Williamson, J. K., and W. H. Hall. 1953. X-ray line broadening from filed aluminium and wolfram Die verbreiterung der roentgen interferenzlinien von aluminium- und wolfram spaenen. *Acta Metall.* 1:22–31.
 36. Juraic, K., D. Garcin, B. Santic, D. Meljanac, N. Zoric, A. Gajovic et al. 2010. GISAXS and GIWAXS analysis of amorphous–nanocrystalline silicon thin films. *Nucl. Instrum. Methods Phys. Res. B* 268:259–262.
 37. Garrido, G. C., B. Pellegrino, P. Ferre, R. Moreno, J. Morante, L. Pavesi et al. 2003. Size dependence of lifetime and absorption cross section of Si nanocrystals embedded in SiO₂. *Appl. Phys. Lett.* 82:1595(1-3).
 38. Wolkin, M. V., J. Jorne, P. M. Fauchet, G. Allan, and C. Delerue. 1999. Electronic States And Luminescence In Porous Silicon Quantum Dots: The Role Of Oxygen. *Phys. Rev. Lett.* 82:197–200.
 39. Lin, G. R., C. J. Lin, C. K. Lin, L. Chou, and Y. Chueh. 2005. Characteristics of constrained ferroelectricity in PbZrO₃/BaZrO₃/PbZrO₃/BaZrO₃ superlattice films. *J. Appl. Phys.* 97:034105–034112.
 40. Kovalev, D., H. Heckler, M. Ben-Chorin, G. Polisski, M. Schwartzkopff, and F. Koch. 1998. Breakdown of k-conservation rule in Si nanocrystals. *Phys. Rev. Lett.* 81:2803–2807.
 41. Hybertsen, M. S. 1994. Excitons in Si nanocrystals. *Phys. Rev. Lett.* 72:1514–1518.
 42. Park, Y. M., Y. J. Park, K. M. Kim, J. C. Shin, J. D. Song, J. I. Lee et al. 2004. State filling phenomena in modulation-doped InAs quantum dots. *J. Cryst. Growth* 271:385–390.
 43. Zhang, P., Y. Feng, X. Wen, W. Cao, R. Anthony, U. Kortshagen et al. 2016. Generation of hot carrier population in colloidal silicon quantum dots for high-efficiency photovoltaics. *Sol. Energy Mater. Sol. Cells* 145:391–396.
 44. Beard, M. C., K. P. Knutsen, P. Yu, J. M. Luther, Q. Song, W. K. Metzger et al. 2007. Multiple Exciton Generation in Colloidal Silicon Nanocrystals. *Nano Lett.* 7:2506–2512.
 45. Govoni, M., I. Marri, and S. Ossicini. 2012. Carrier multiplication between interacting nanocrystals for fostering silicon-based photovoltaics. *Nat. Photonics* 6:672–679.
 46. Weickert, J., R. B. Dunbar, H. C. Hesse, W. Wiedemann, and L. Schmidt-Mende. 2011. Nanostructured Organic and Hybrid Solar Cells. *Adv. Mater.* 23:1810–1828.
 47. Chen, L-M., Z. Hong, G. Li, and Y. Yang. 2009. Recent Progress in Polymer Solar Cells: Manipulation of Polymer: Fullerene Morphology and the Formation of Efficient Inverted Polymer Solar Cells. *Adv. Mater.* 21:1434–1449.